Atmospheric Environment 278 (2022) 119074

Contents lists available at ScienceDirect

Atmospheric Environment

journal homepage: www.elsevier.com/locate/atmosenv

Impacts of large-scale deployment of mountainous wind farms on wintertime regional air quality in the Beijing-Tian-Hebei area

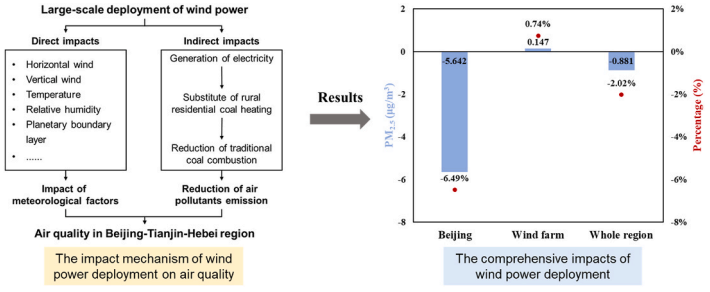
Ziwen Ruan [a,c], Xi Lu [a,b,c,*], Shuxiao Wang [a,c], Jia Xing [a,c,**], Wei Wang [d], Dan Chen [e,***], Chris P. Nielsen [f], Yong Luo [g], Kebin He [a,b,c], Jiming Hao [a,c]

[a] Beijing Laboratory of Environmental Frontier Technologies, School of Environment, Tsinghua University, Beijing, 100084, China
[b] Institute for Carbon Neutrality, Tsinghua University, Beijing, 100084, China
[c] State Key Joint Laboratory of Environment Simulation and Pollution Control, Tsinghua University, Beijing, 100084, China
[d] National Center for Atmospheric Research, Boulder, CO, USA
[e] Institute of Urban Meteorology, Chinese Meteorological Administration, Beijing, China
[f] Harvard John A. Paulson School of Engineering and Applied Sciences, Harvard University, Cambridge, MA, USA
[g] Ministry of Education Key Laboratory for Earth System Modeling, Department of Earth System Science, Tsinghua University, Beijing, China

HIGHLIGHTS

- Direct and indirect wind power deployment effects on air quality were evaluated.
- Integrated frame treating wind extracting and emission substituting is established.
- Direct impacts are generally negligible but occasionally worsen in polluted days.
- Indirect impacts by substituting rural heating significantly improved air quality.
- Compressive evaluation should be taken into account to support energy policies.

GRAPHICAL ABSTRACT



The impact mechanism of wind power deployment on air quality

The comprehensive impacts of wind power deployment

ARTICLE INFO

Keywords:
Wind power
$PM_{2.5}$
WRF-CMAQ
Meteorological impacts
Indirect benefits
Comprehensive impacts

ABSTRACT

The development of wind power plays an essential role in achieving China's carbon neutrality goals and air quality standards. A large number of studies have addressed the benefits of substituting fossil fuels with wind power on climate and air quality (defined as indirect impact) by macro-scale methodology. In recent years, more and more researchers have discussed its impacts on the general atmospheric circulation and air pollution dispersion (defined as direct impact) by parameterizing wind energy extraction in meso-micro scale models. However, the comprehensive investigation (considering both direct and indirect impacts) of the utilization of wind power on atmosphere environmental impacts remains vacant. Our study first evaluated both the direct and indirect impacts of wind power on air quality through an integrated methodological framework by using WRF-CMAQ system. The present analysis took wind farms located in Zhangjiakou to explore their impacts on air quality in winter, particularly over the downwind Beijing municipal area in the North China Plain. Results indicated that the deployment of wind power leads to spatially mixed direct impacts on $PM_{2.5}$ concentrations in

* Corresponding author. Beijing Laboratory of Environmental Frontier Technologies, School of Environment, Tsinghua University, Beijing, 100084, China
** Corresponding author. Beijing Laboratory of Environmental Frontier Technologies, School of Environment, Tsinghua University, Beijing, 100084, China
*** Corresponding author.
E-mail addresses: xilu@tsinghua.edu.cn (X. Lu), xingjia@tsinghua.edu.cn (J. Xing), dchen@ium.cn (D. Chen).

https://doi.org/10.1016/j.atmosenv.2022.119074
Received 14 November 2021; Received in revised form 14 March 2022; Accepted 19 March 2022
Available online 23 March 2022
1352-2310/© 2022 Elsevier Ltd. All rights reserved.

Beijing with a monthly net increase of 0.067 μg/m^3 (0.08%) relative to the regional average. Contrarily, the substitution of coal-burning with wind power in rural household heating would result in notable indirect benefits to monthly $PM_{2.5}$ concentrations in Beijing, specifically, reducing emissions of CO_2 and conventional air pollutants by 64% in rural heating sector. The combined impacts of wind power displayed regional differences: in the wintertime (January), Zhangjiakou $PM_{2.5}$ concentrations increased (+0.147 μg/m^3) whereas, decreases are achieved (−5.642 μg/m^3) in Beijing. Therefore, to support the large-scale deployment of wind power, future energy policies should take comprehensive account of the diverse environmental impacts, including both the indirect benefits of fossil energy substitution and the potential direct atmospheric effects on regional air quality.

1. Introduction

Over past three decades, China was dominated by coal-fired power industry in energy structure which cause severe air pollution and carbon emission. To solve the severe haze pollution in the nationwide, although great achievements have been made in the end-of-pipe pollution control, the clean energy still is expected to have great development in the energy supply side (Lu et al., 2020). Wind power has witnessed rapid development in China since the Renewable Energy Law of China was promulgated in 2005. The total installed wind capacity of China expanded from 1.26 GW in 2005 to 281 GW in 2020 (Zhang et al., 2020). According to the Global Wind Report (2021), China has evolved into the largest wind power market in the world, and installed capacity will reach 800 GW by 2030 and 3000 GW by 2060. The development of wind energy in China is a necessary measure that serves two purposes: one, to transition its energy system to a low-carbon alternative, and secondly to cope with the dual challenges of global climate change and domestic air pollution. Recently, China further committed to 1200 GW of wind and solar installed capacity and a 25% share of non-fossil fuels in the primary energy consumption by 2030 (Xi, 2020). With the cost of wind-generated electricity gradually becoming equal to or even lower than power from coal-fired plants (Tu et al., 2019), wind power is expected to play an increasingly important role in future energy services in China. Under these circumstances, a comprehensive understanding of the impacts of wind power has become imperative to guide its future sustainable development.

Wind power can impact the climate system and air quality through two channels: firstly, reducing anthropogenic emissions of both CO_2 and air pollutants by replacement of fossil fuels (hereafter regarded as indirect impacts) (Ma et al., 2013; Nordman and Vandermolen, 2014; Yang et al., 2017), and secondly, by affecting meteorological conditions both locally or downstream by extracting kinetic energy from the air flows (hereafter regarded to as direct impacts) (Fitch et al., 2012; Keith et al., 2004; Li et al., 2018; Miller and Keith, 2018). A large body of literature has addressed the indirect benefits through Life Cycle Assessment (LCA), with consistent results showing that development of wind power results in evident reductions in emissions of CO_2 and air pollutants, from a life-cycle perspective (Li et al., 2019a; Raadal et al., 2014; Xu et al., 2018). In addition, part of the research used the calculation method of emission factors to discuss the co-benefits of CO_2, air pollutants, and water resources utilization brought by wind power (Ma et al., 2013; Yang et al., 2017).

The direct impacts of the deployment of wind power on climate have also attracted attention in more recent studies. Miller and Keith (2018) have comprehensively reviewed the existing articles discussing the direct climate impacts through observation methods (both satellite-based and ground-based observations). A large number of ground observation experiments though wind tower observation data, surface flux tower, lidars, radiometer and other measurement methods have shown that the deployment of wind power can decreased wind speeds and have impacts on the local and downwind temperature, moisture, heat transfer flux, and other meteorological conditions (Rajewski et al., 2013, 2014; Roy and Traiteur, 2010; Smith et al., 2013). Archer et al. (2019) recently conducted vertical mixing measurement (VERTEX) campaigns, measuring changes in near-surface properties by wind turbines, which corrected the explanation of surface temperature effects stated by Roy and Traiteur (2010) and demonstrated the complexity impacts of the wind turbine operation. Additionally, by using satellite observation data, Zhou et al. (2012) further suggested that the deployment of wind turbines in Texas could increase the surface temperature by 0.72 °C per decade in a local wind farm region based on satellite data from 2003 to 2011. Subsequent studies (Harris et al., 2014; Zhou et al., 2013) through satellite observation data also confirmed that wind farms bring a certain degree of warming at night locally in plain regions, because the operated wind-turbine rotors enhance vertical mixing, disturb the surface inversion layer, and transfer warming air to surface during nighttime. These researches are consistent with the relevant conclusions obtained from ground observation experiments (Slawsky et al., 2015; Walsh-Thomas et al., 2012; Xia et al., 2016).

To overcome the limitations of observational data in both spatial coverage and vertical profiles, several scholars adopted numerical general circulation models with adjusted surface drag coefficients or other wind farm parameterization (WFP) to quantify the impacts of wind farms (Fitch et al., 2012; Keith et al., 2004; Li et al., 2018), which revealed more details in both unfavorable and favorable directions for climate impacts. Through global model simulation, a study by Keith et al. (2004) showed that the direct consequences of large-scale wind development on climate are much less than the carbon reduction benefits, while a study by Li et al. (2018) further demonstrated that extensive installation of wind farms in Sahara desert areas could increase local precipitation and vegetation coverage. Fitch et al. (2012) expanded the wind farm calculation method of Blahak et al. (2010) and developed a new WFP in the Weather Research and Forecasting Model (WRF). Fitch et al. (2013) applied the WFP-WRF to simulate wind-farm impacts for a region of the U.S. Midwest in Kansas with results suggesting that wind farms may decrease horizontal wind speeds by up to 80 km downstream, especially under stable conditions at night, but that they may also enhance vertical mixing (at altitudes of 500–1000 m).

Wind farm-perturbed meteorology could change the distribution of air pollution, particularly in population-dense downstream cities, which is a growing concern in air quality management. A study coupled meteorology and atmospheric chemistry model WRF-Chem by Mo et al. (2017) indicated that the operated wind farm would cause increased nitrogen dioxide (NO_2) concentration in the immediate upstream and the edge of the wind farm, but lower NO_2 concentration within the wind farm, because of the changes of wind speed in the internal boundary layer and the enhancement of surface roughness length over the wind farm. Besides, Li et al. (2020) also demonstrated that the evident direct $PM_{2.5}$ concentration impacts the establishment of large-scale wind farms in Northern China.

In summary, the comprehensive impacts of air pollutants on the deployment of wind power, including both the direct impacts caused by meteorological changes and the indirect benefits brought about by the substitution of fossil fuels, have not yet been sufficiently addressed in the existing literature. The present study intends to evaluate the impacts of the deployment of wind power on air quality through an integrated methodological framework (Fig. 1A). The domain of 38.27°–41.67° N latitude and 113.08°–118.01° E longitude selected for this analysis covers the Chinese capital environs located in the Beijing-Tianjin-Hebei (BTH) area, where heavy pollution episodes frequently occur in winter.

Here, we focus on impacts from the deployment of wind power in Zhangjiakou (ZJK) for two reasons: (1) a large number of wind farms have already been constructed or will be constructed in ZJK (Zhang et al., 2021) to supply green electricity for the 2022 Beijing Winter Olympic Games; (2) ZJK is located upstream in the prevailing northwesterly winds associated with Beijing air pollution removal processes in winter (Chang et al., 2019; Li et al., 2019b). Thus, evaluating the impacts of wind power deployment on meteorological conditions also has practical importance for Beijing's air quality management (Fig. 1B).

2. Material and methods

We couple a mesoscale-meteorology model (WRF) with an air quality model (Community Multiscale Air Quality model, CMAQ) and a high-resolution 1-km emission inventory developed by Tsinghua University (Byun and Ching, 1999; Skamarock et al., 2008; Zheng et al., 2019). The WRF-CMAQ system is employed to explore the interactions between meteorological conditions and aerosols, and resulting impacts on air pollutant concentrations. In addition, this system was widely applied in the researches of the interaction of airborne aerosols and meteorological factors (Tao et al., 2021; Wang et al., 2014, 2022), the components of secondary air pollutants (Hu et al., 2016a, 2016b), transmission factors of air pollutants source (Chang et al., 2019; Zheng et al., 2019), atmospheric environmental impacts of government policies (Hu et al., 2021; Zhao et al., 2018, 2021), etc.

In this study, we focus on investigating the impacts of the deployment of wind power with a total capacity of 16 GW in ZJK (the level currently planned for 2030) compared to a reference scenario with no deployment of wind power (the base scenario in Table 1). In addition, scenarios of 8 GW (current capacitance) and 32 GW (expected capacitance in 2050) in ZJK are also examined in the Supplementary Information. Using the WFP scheme in the WRF simulation, we assume that 8000 2-MW wind turbines potential installations at a density of 2 MW/km^2 in the square region shown in Fig. 1B. The indirect impacts from the deployment of wind power are evaluated relative to Beijing rural residential sector with the substituted emissions subtracted from 16-GW scenario in Table 1.

2.1. Study region and duration

As illustrated in Fig. S1, we designed two nested domains without nudging technique both in the meteorology and air quality simulations with the horizontal grid cell numbers of 255 × 243 and 399 × 399, and horizontal resolutions of 3 km and 1 km, respectively. The simulation domain includes Beijing, Tianjin, and a part of Hebei province. The boundary condition and initial concentration for the 1-km simulation are updated with the results from the 3-km simulation to ensure the simulation of regional transmission (Tao et al., 2018, 2019). The vertical resolution includes 27 levels (up to 100 mbar) of which 12 are below 1 km with 4 intersecting the wind turbine's rotor area.

We chose January 1–31 in 2015 as the study timeframe, to focus on the most polluted month in the BTH area. And the simulation period is from December 27 in 2014 to January 31 in 2015, because the first 5 days were used to spin up in the CMAQ model. In order to reduce the "chaos seeding" of numerical model (Ancell et al., 2018), we chose the WRF results of 24–48 h in the middle of each 3-day simulation for the final meteorological analysis and the input of CMAQ model. This means that in the 31-day analysis, we simulated 3-day simulations, 31 times in WRF. In addition, based on the results of Base scenario, we divided three concentration levels in Table 1 to analyze direct $PM_{2.5}$ changes in results part.

2.2. Model configuration

We applied in this study the mesoscale numerical WRF model (version 3.7) developed by the National Centre for Atmospheric Research (Skamarock et al., 2008). This model is appropriate for the regional simulation implemented here. We used Moderate-Resolution Imaging Spectroradiometer (MODIS) products for the land use data, and the Final Operational Global Analysis (FNL) data from the National Center for Environmental Prediction (NCEP) for the boundary input data. These NCEP FNL data are on 1-degree by 1-degree grids prepared operationally every 6 h from the Global Data Assimilation System (GDAS).

The main selected physical schemes (Table 2) include version 2 of the Kain-Fritsch cumulus (Kain and Kain, 2004) cloud parameterization, the WRF Single-Moment 6-class scheme (Hong and Lim, 2006) for the Microphysics process, and the Rapid Radiative Transfer Model for GCM (RRTMG) scheme (M. J. Iacono et al., 2008) for the radiation process in our study. Referring to the WRF manual, we applied the Mellor–Yamada–Nakanishi–Niino (MYNN) level 2.5 PBL scheme, supported by WFP calculation (Nakanishi and Niino, 2009). In addition, we choose

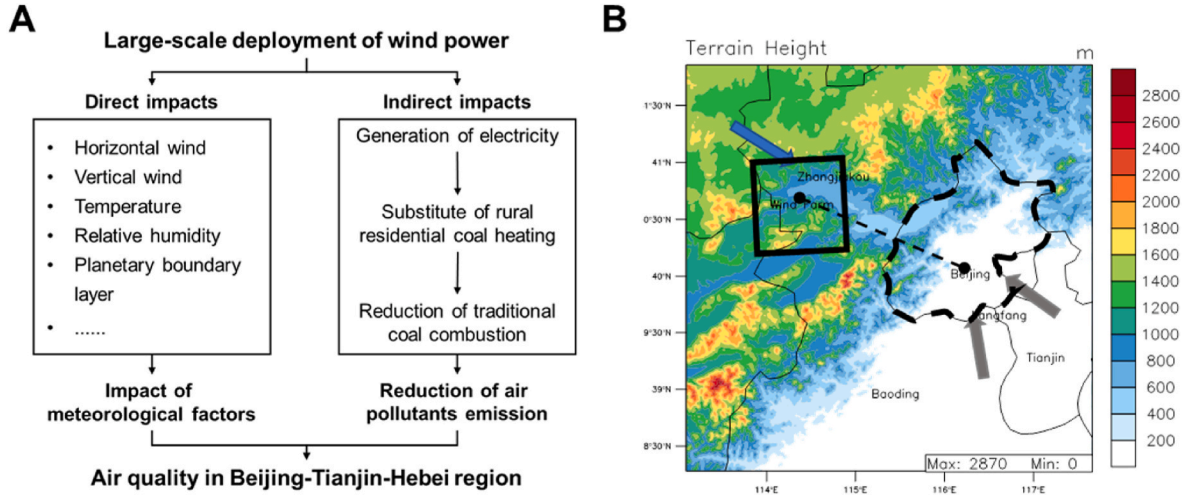


Fig. 1. The response of meteorological factors, air pollutants emission and air pollutants concentration: (A) The flow chart of the impact mechanism of the deployment of wind power. **(B)** The research domain and the wind farm's location overlain with the terrain height. The black rectangle with solid lines represents the location of the wind farms, the black dotted curves (boundary) illustrate the area of the capital, Beijing. The black dotted line is the straight section from the wind farms to Beijing, the blue arrow is the main removal wind direction, and the grey arrows are the main pollutants accumulation direction. (For interpretation of the references to color in this figure legend, the reader is referred to the Web version of this article.)

Table 1
Scenarios and the concentration criteria under different $PM_{2.5}$ pollution levels.

Scenario name	Wind farm parameter	Installed capacity	Installed density	Description of anthropogenic emission.
Base	no	–	–	2015 emission inventory.
8-GW	yes	8 GW	1 MW/km^2	2015 emission inventory.
16-GW	yes	16 GW	2 MW/km^2	2015 emission inventory.
32-GW	yes	32 GW	4 MW/km^2	2015 emission inventory.
Indirect impacts	yes	16 GW	2 MW/km^2	According to relevant policies of electric energy substitution in BTH region (Wang et al., 2020). We suppose wind power used in the residential sectors. Substitute of Beijing rural heating pollutants in 2015 emission inventory.
Levels	**Concentration (μg m^{-3})**	**Dates in January 2015**		
Clean	$PM_{2.5} < 75$	1, 2, 6, 7, 9, 10, 11, 16, 18, 19, 21, 24, 27, 28, 29, 30, 31		
Moderate pollution	$75 \leq PM_{2.5} < 150$	5, 8, 12, 17, 20, 22, 23, 25, 26		
Heavy pollution	$150 \leq PM_{2.5}$	3, 4, 13,14, 15		

Table 2
Main physics parameterizations used in the WRF model.

Physics process	Parameterizations schemes
Microphysics	Single-Moment 6-class scheme
Longwave/Shortwave Radiation	Rapid Radiative Transfer Model for GCM
Surface Layer	Nakanishi and Niino PBL's surface layer scheme
Land Surface	Noah Land-Surface model
Urban Surface	Urban canopy model
Planetary Boundary layer	Mellor-Yamada Nakanishi and Niino Level 2.5 PBL
Cumulus Parameterization	Kain-Fritsch scheme

the Noah Land Surface Model for the land surface scheme with improved performance in forecasting low-level temperature and humidity in mesoscale meteorological models (Ek et al., 2003).

CMAQ is a regional model developed by the United States Environmental Protection Agency (Byun and Ching, 1999) and is widely used in air quality forecasting and evaluation. To couple the WRF-CMAQ modeling system, we converted the output data files from WRF to the input format from CMAQ using Meteorology-Chemistry Interface Processor version 4.2 (Byun et al., 1999). For the chemical processes in CMAQ, we adopted the latest chemical mechanism CB6 including the aerosol reaction mechanism AERO6. The input anthropogenic emission data used in this research is from ABaCAS (Ding et al., 2019; Wang et al., 2013; Zheng et al., 2019) which cover the entire China region including eight pollutants: SO_2, NO_x, CO, VOCs, PM_{10}, $PM_{2.5}$, black carbon (BC), and organic carbon (OC) with a horizontal resolution of 1 km (Tao et al., 2019).

2.3. Wind turbines configuration

We applied the updated WFP scheme (Archer et al., 2020; Fitch et al., 2012) in the WRF model (Table 3), an approach that was widely adopted in recent studies (Wang et al., 2019a, 2019b). By applying the power and thrust curves of the wind turbines, this scheme can calculate the impacts of mesoscale simulation. Similarly, this scheme can also express the extracted energy and the effective physical parameters of wind farms in the complex terrain (Wang et al., 2019a, 2019b; Yang et al., 2018). The idealized wind farm scenarios in our study are summarized in Table 1. The power curves for the wind turbines used in our research are based on Vestas V90–2.0 MW, with a nominal power output of 2.0 MW, 95 m hub-height, 105 m rotor diameter, 3.5 m/s cut-in, 25 m/s cut-out, and 12 m/s rated wind speeds (Fig. 2).

2.4. Model performance

The performance of the simulation using the WRF-CMAQ model was evaluated by comparing the baseline scenario with the observed concentration of pollutants (Fig. 2). The observation data (OBS) of the meteorological parameters were taken from the National Climate Data

Table 3
Wind farm parameterization scheme in WRF.

Variable	Variable definitions	Calculation Formula
C_T	**Thrust coefficient**: the drag coefficient of wind turbines to extract kinetic energy (KE) from atmosphere.	C_T and C_P obtained from the turbine manufacturer.
C_P	**Power coefficient**: a fraction of total kinetic energy from atmosphere converted into electrical energy.	
C_{TKE}	The fraction of energy converted into Turbulent Kinetic Energy (TKE).	$C_{TKE} = C_T - C_P$
F_{drag}	The force of drag induced by a wind turbine on the impinging flow	$F_{drag} = \frac{1}{2}C_T(\lvert V\rvert)\rho\lvert V\rvert VA$, where $V=(u,v)$ is the horizontal velocity vector, ρ is the air density, A is the cross-sectional rotor area.
$\frac{\partial KE_{cell}^{ijk}}{\partial t}$	The rate of change of KE within grid cell.	$\frac{\partial KE_{cell}^{ijk}}{\partial t} = \rho_{ijk}\lvert V\rvert_{ijk}\frac{\partial \lvert V\rvert_{ijk}}{\partial t}(z_{k+1}-z_k)\Delta x\Delta y$, where i, j, k are the number of grids in three-dimensional, Δx and Δy are the horizontal grid spacing and z_k is the height of vertical coordinate.
$\frac{\partial \lvert V\rvert_{ijk}}{\partial t}$	The rate of change of horizontal velocity vector within grid cell.	$\frac{\partial \lvert V\rvert_{ijk}}{\partial t} = -\frac{\frac{1}{2}N_t^{ij}C_T(\lvert V\rvert_{ijk})\lvert V\rvert_{ijk}^2 A_{ijk}}{(z_{k+1}-z_k)}$, where N_t^{ij} is horizontal density of wind turbines in grid cell.
$\frac{\partial u_{ijk}}{\partial t}$	The horizontal momentum tendency terms of horizontal u component.	$\frac{\partial u_{ijk}}{\partial t} = \frac{u_{ijk}}{\lvert V\rvert_{ijk}}\frac{\partial \lvert V\rvert_{ijk}}{\partial t}$
$\frac{\partial v_{ijk}}{\partial t}$	The horizontal momentum tendency terms of horizontal v component.	$\frac{\partial v_{ijk}}{\partial t} = \frac{v_{ijk}}{\lvert V\rvert_{ijk}}\frac{\partial \lvert V\rvert_{ijk}}{\partial t}$
$\frac{\partial P_{ijk}}{\partial t}$	The rate of extracted useful electrical energy by turbines within grid cell.	$\frac{\partial P_{ijk}}{\partial t} = \frac{\frac{1}{2}N_t^{ij}C_P(\lvert V\rvert_{ijk})\lvert V\rvert_{ijk}^3 A_{ijk}}{(z_{k+1}-z_k)}$
$\frac{\partial TKE_{ijk}}{\partial t}$	A fraction of power extracted by the turbines converted into TKE.	$\frac{\partial TKE_{ijk}}{\partial t} = \frac{\frac{1}{2}N_t^{ij}C_{TKE}(\lvert V\rvert_{ijk})\lvert V\rvert_{ijk}^3 A_{ijk}}{(z_{k+1}-z_k)}$
P_{ijk}	The power output of the wind turbines per unit mass.	$P_{ijk} = \frac{1}{2}N_t^{ij}\Delta x\Delta y C_P\rho_{ijk}\lvert V\rvert_{ijk}^3 A_{ijk}$

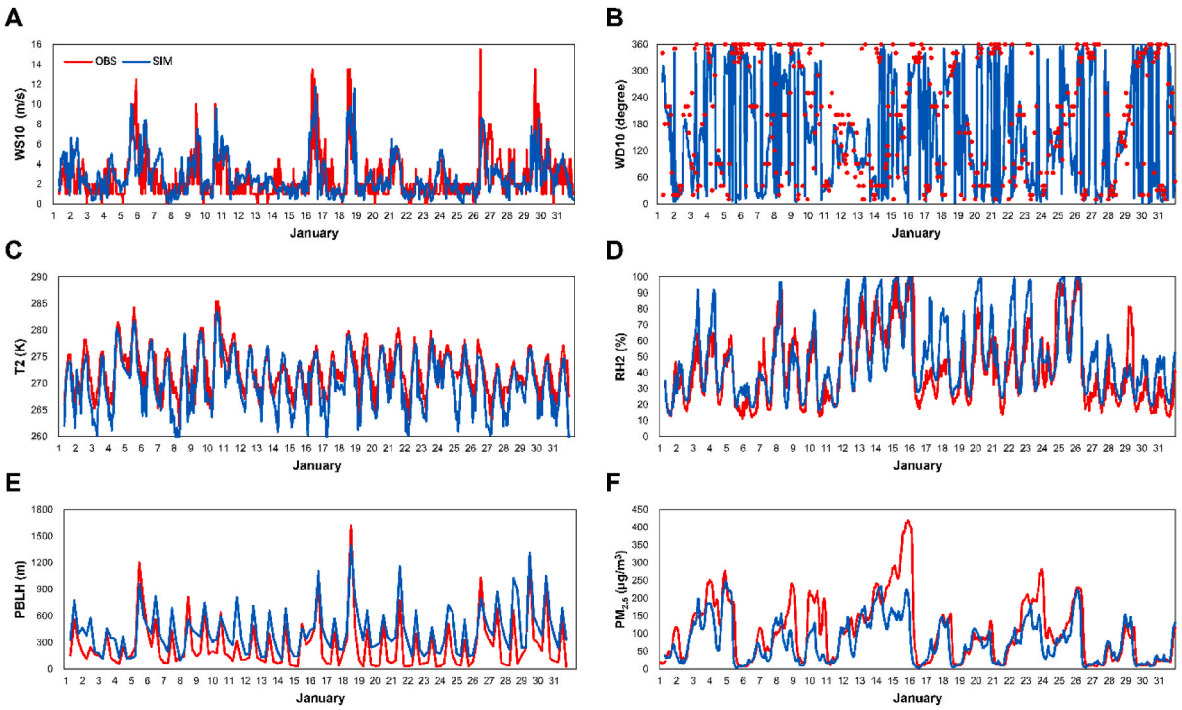


Fig. 2. Time series of observed and simulated meteorological parameters and $PM_{2.5}$ concentrations in Beijing region. (A) WS10 – wind speed at 10 m. **(B)** WD10 – wind direction at 10 m. **(C)** T2 – temperature at 2 m. **(D)** RH2 – relative humidity at 2 m. **(E)** PBLH – planetary boundary layer height. **(F)** concentration of $PM_{2.5}$.

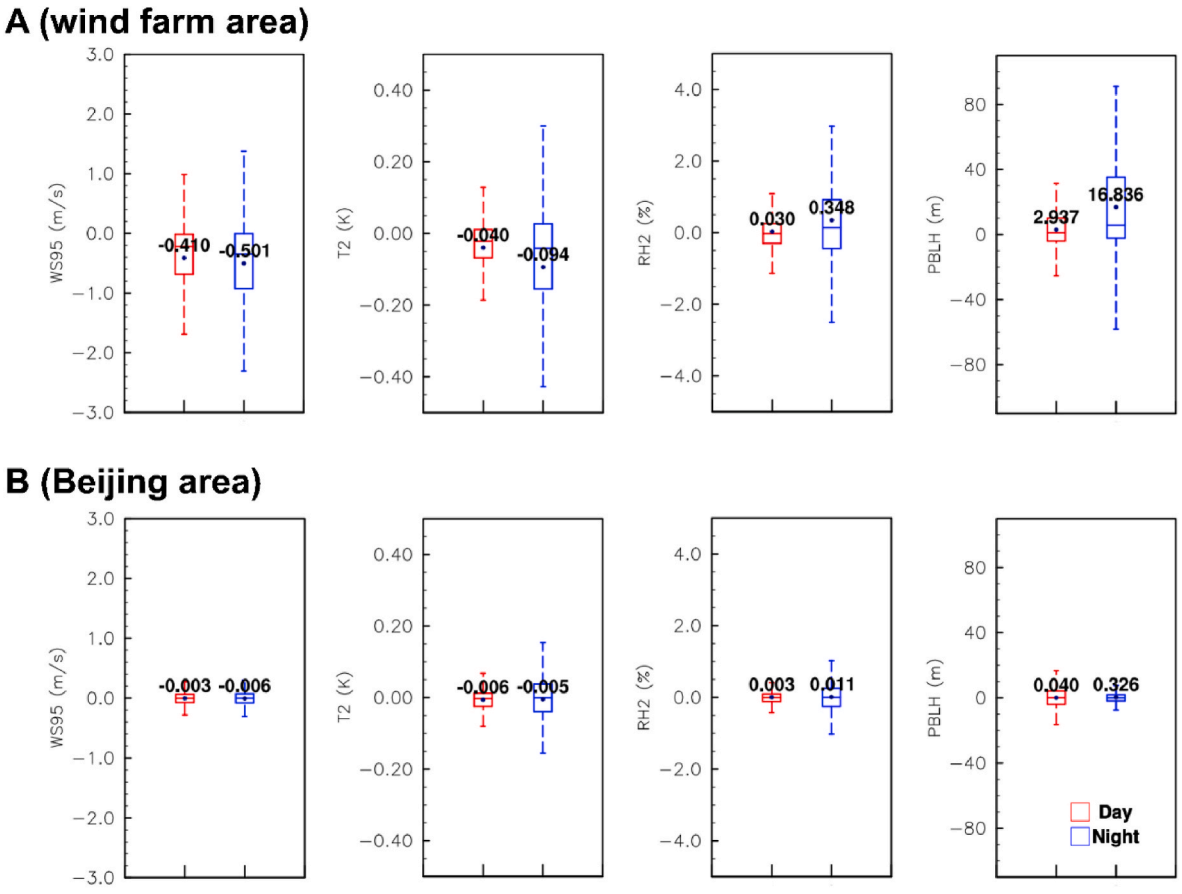


Fig. 3. Changes of different physical parameters in wind farm (A) and Beijing (B) area. (A) and (B) show contributions in WS95 (m/s), T2 (K), RH2 (%) and PBLH (m). The red/blue box plots represent daytime/nighttime respectively. Each box plot indicates a range of changes including six values: 1st percentile (endpoint of low whisker), 25th percentile (bottom of box), median (dot), mean (center line in box), 75th percentile (top of box), and 99th percentile (endpoint of high whisker). (For interpretation of the references to color in this figure legend, the reader is referred to the Web version of this article.)

Centre (NCDC, https://www.ncdc.noaa.gov/data-access), with the $PM_{2.5}$ OBS derived from the China National Environmental Monitoring Center with 56 air-quality stations in this region, including 35 in Beijing (the location of these sites shown in Fig. S1). We summarized the model performance in predicting the meteorological variables, including wind speed, wind direction, temperature, relative humidity, and air pollutant $PM_{2.5}$ (Table S1) (Boylan and Russell, 2006; Chen et al., 2016; Emery et al., 2001; Environmental Protection Agency U.S, 2007; Tao et al., 2019). The error of meteorological simulation in our research is similar to that of other studies (Chen et al., 2016; Tao et al., 2019), so these results can be used for analysis and air quality simulated input files. Referring to the benchmark for air pollutants proposed by Boylan and Russell (2006) and the U.S. Environmental Protection Agency (2007), the model performance in simulating $PM_{2.5}$ is acceptable.

3. Results

3.1. Direct impacts on regional meteorology

As illustrated in Fig. 3A and B, the meteorological impacts from the development of 16-GW wind power tend to be stronger in the local wind farm region than the downstream Beijing area in terms of hub-height wind speed (WS95), 2-m temperature (T2), 2-m relative humidity (RH2), and the planetary boundary layer height (PBLH). By directly extracting kinetic energy from the air flow, wind turbine operation causes the onsite horizontal wind speed (WS95) to decrease by 0.410 m/s during daytime (14:00–16:00 Local Standard Time, LST) and by 0.501 m/s during nighttime (22:00–4:00, LST) on a monthly average. In contrast, the impacts on monthly average WS95 in the Beijing area, 120 km downwind of the windfarm site, are negligible, decreasing by only 0.003 m/s during the daytime and by 0.006 m/s during nighttime.

The results also suggest that the deployment of wind power in the mountainous areas of ZJK has a cooling impact on surface temperatures (T2) in both daytime and nighttime. These results differ from the satellite observations reported for the plains region of Texas (Zhou et al., 2012), in which case, wind farms observed to have a warming effect on surface temperature, particularly in the nighttime in winter due to the original stable inversion layer and the influence on vertical heat transfer processes. In the case of the mountainous area in the present analysis, by analyzing changes in wind speed in the valley (Fig. S5), we attribute the cooling effect in the valley to the superimposed effect of the valley wind and the increase ground wind brought by the wind turbines. An explanation for this is that the wind turbines accelerate the flow of ground cooling wind from the hillside towards the valley, strengthening mountainous circulation at surface level; and consequently, decreasing valleyed temperatures during the nighttime. Along with the cooling temperature and decreased wind speeds, the RH2 tends to increase by 0.03% during daytime and 0.348% during nighttime in the wind farm area.

In the vertical direction, the operation of wind turbines results in an average increase in the PBLH of 2.937 m during daytime and 16.836 m at night in wind farm areas, and 0.040 m during the day and 0.326 m during the night in Beijing areas. During the nighttime, the influence on the PBLH can reach further downstream, impacting cities in the plains surrounding Beijing (Fig. S4). The primary reason for the changes of the PBLH relates to the large fluctuations in circulation patterns (Fig. S6), including more active vertical motion, leading to increasing vertical mixing up to 3–4 km (above sea level) in the wind farm area, and up to 1.5–2 km (above sea level) in the Beijing area. These results imply that the rotation of the wind turbines can disrupt the stable vertical thermodynamic structure even above the PBLH, consequently enhancing the vertical mixing of the airflow.

A positive correlation exists between turbulent kinetic energy (TKE) and the PBLH in terms of the diurnal cycle. As illustrated in Fig. 4A and

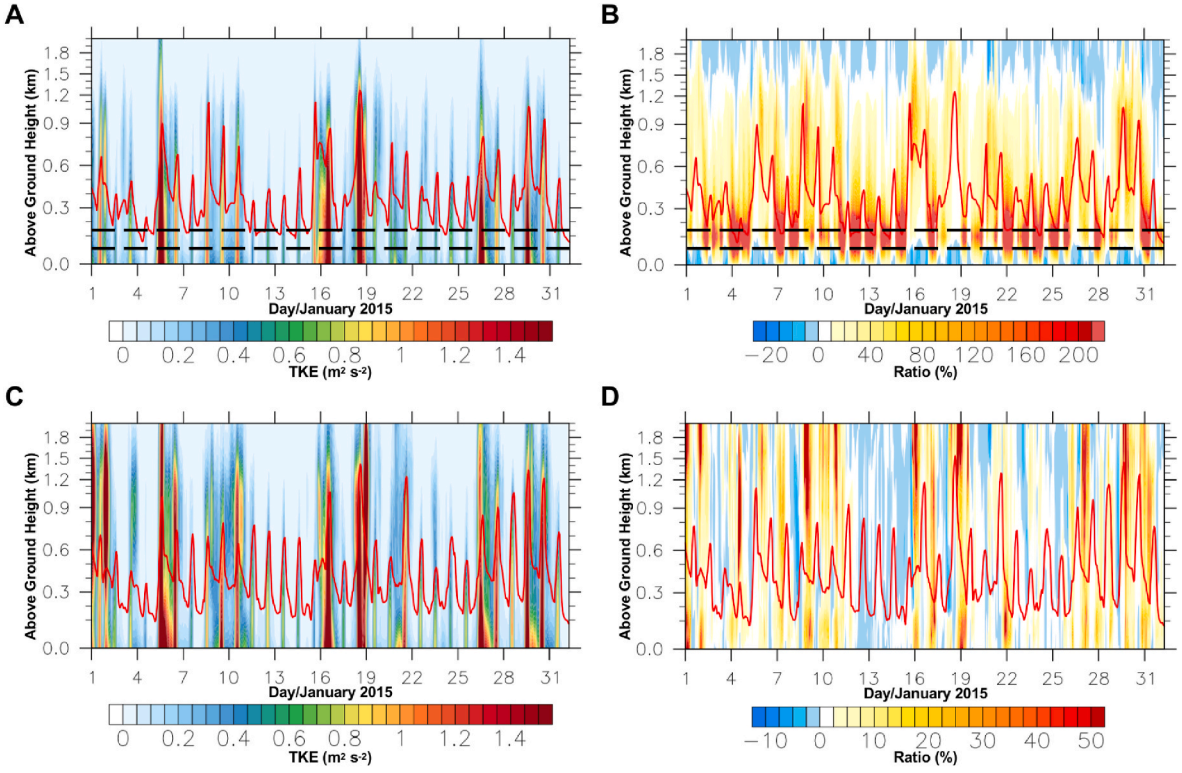


Fig. 4. The time-height diagram of TKE (color spectrum) and PBLH (red line) for the wind farm area (A) and Beijing area (C) in the base scenario. The ratio of the 16-GW to base scenarios for TKE (color spectrum) and perturbed PBLH (red lines) in the 16-GW scenario for the wind farm area (B) and Beijing area (D). The dashed lines in (A) and (B) represent the heights swept by the wind turbines in the wind farm area. (For interpretation of the references to color in this figure legend, the reader is referred to the Web version of this article.)

C, the peaks of TKE and PBLH occur coincidently during daytime in both the wind farm and Beijing areas. The maximum height swept by the wind turbine blades (150 m) tend to exceed the original PBLH at nighttime (Fig. 4A), facilitating the transfer of the wind-turbine-generated TKE to heights above the original PBL. The results in Fig. 4B indicate increases in TKE of 100%–200% above the original PBLH during nighttime. This increase, in turn, strengthens the vertical mixing and the PBLH in the wind farm area, consistent with the findings reported for wind farms in the Midwest plains region of the U.S. (Fitch et al., 2013) and the hilly plateau region in Zhangbei located in the north of ZJK (Wang et al., 2019a). In contrast, wind turbines operate well below the PBLH during the daytime, and therefore the TKE produced by wind turbines has a limited impact on the original intense turbulence within the PBL. As a result, the PBLHs in the wind farm area of ZJK increase slightly in the 16-GW scenario during the daytime. It is worth noting that the changes of PBLH exhibit a complex distribution (Fig. S6), reflecting the spatial-heterogeneous influences associated with the valley circulation in the mountainous terrain where the wind turbines are located.

Differing from the results for wind farms located in plain terrain, where the increase of TKE occurs locally (Fitch et al., 2012, 2013), Fig. 4D indicates that the 16-GW scenario leads to evident increases of TKE, particularly at high altitudes, in the downstream Beijing area during nighttime. The higher TKE reflects the fact that the wind turbines are located in ZJK at elevations approximately 1 km higher than the Beijing area. The perturbation of wind turbines can strengthen the TKE up to 2 km above ground in the wind farm area, which results in extended impacts on downstream regions through the regional atmospheric circulation.

3.2. Impacts on air quality

Fig. 5 illustrates the direct impacts on $PM_{2.5}$ concentrations driven by the operation of wind turbines in ZJK during daytime (14:00–16:00, LST) and nighttime (22:00–4:00, LST) for clean, moderate, and heavy pollution days (as differentiated in Table S3), as well as monthly average conditions. Results show that the general impacts on the spatial distribution of $PM_{2.5}$ are relatively strong during nighttime, with monthly concentrations increasing by 0.063 μg/m^3 (0.40%) as compared with 0.035 μg/m^3 (0.24%) during daytime for the entire study domain (Fig. 5B). As discussed earlier, the operation of wind turbines has a larger impact on wind speeds and relative humidity during nighttime

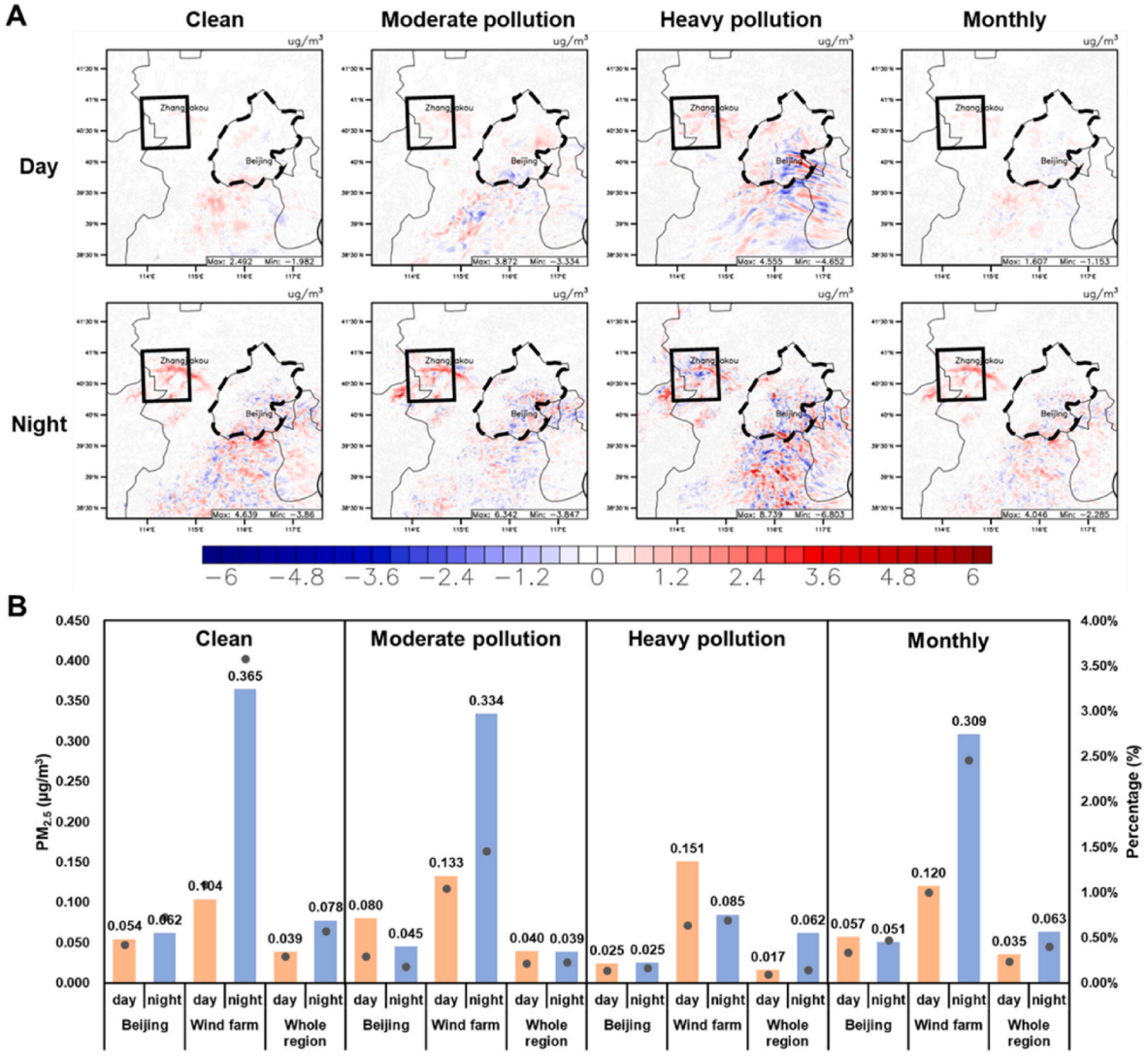


Fig. 5. The impact of 16 GW of wind farms on $PM_{2.5}$ concentrations: the spatial distribution (A) and absolute values and percentages (B) of changes in $PM_{2.5}$ concentrations for the designated region. In (A), the square region designated by solid black lines represents the location of the wind farms and the region outlined in black dashed curves represents the location of Beijing. In (B), columns show the absolute changes in $PM_{2.5}$ concentrations, grey dots the percentage changes in total $PM_{2.5}$ concentrations, and "whole region" refers to the entire domain shown in (A).

when compared to daytime, leading to favorable conditions for the formation of pollution. In addition, the increase of PBLH (Fig. 3) tends to facilitate the diffusion of air pollution, especially during nighttime. However, as indicated by the $PM_{2.5}$ diurnal cycle, within the nighttime boundary layer, formation process (instead of dispersion and transport processes) is dominating the $PM_{2.5}$ concentration. Thus, the favorable change of pollutants vertical diffusion is relatively weaker than the unfavorable change of formation caused by decreased wind and increased humidity, which leads to overall increased $PM_{2.5}$ concentration during nighttime. The meteorology-driven increase in $PM_{2.5}$ concentration is particularly evident in the wind farm area, where the monthly average value was increased by 0.120 μg/m^3 (1.00%) during daytime and by 0.309 μg/m^3 (2.46%) during nighttime.

The impact on $PM_{2.5}$ in the downstream Beijing area demonstrates a complex spatial distribution with a slight monthly average increase (0.057 μg/m^3 or 0.34% during daytime, and 0.052 μg/m^3 or 0.47% during nighttime). At night during heavy pollution episodes, the average increase in $PM_{2.5}$ concentrations amounted to only 0.17% over the Beijing area, much lower than the values (0.73%) for clean periods. There is speculation that the increment of PBLH facilitates the vertical mixing processes at nighttime during heavy pollution events, which leads to more potent dilution effects when compared to clean air periods. The phenomenon reflects tradeoffs between enhanced vertical mixing and decreased advection in the Beijing area, both of which are impacted by the operation of wind farms in ZJK.

During the daytime, the influence of wind farms on $PM_{2.5}$ tends to be weaker during heavy pollution periods (0.14% in Beijing, 0.64% in wind farm area) than clean periods (0.42% in Beijing, 1.09% in wind farm area), since the increased vertical mixing of wind turbines increases the diffusion of $PM_{2.5}$ during the relatively static daytime periods. However, it is to note that the changes in $PM_{2.5}$ concentration increased by 0.104 μg/m^3 during clean periods and by 0.151 μg/m^3 during heavy pollution periods in the wind farm area. These differences are attributed to the fact that when the $PM_{2.5}$ concentrations are high, the effects from meteorological perturbations tend to be amplified.

The Action Plan of the "blue sky defense battle" vigorously promotes fuel shifting from coal to electricity or natural gas for rural household heating in Beijing. Thus, we further analyzed the indirect impacts of generated wind power on air quality improvement through the replacement of rural residents using coal for heating. The power outputs of wind farms were derived by WRF simulation, and the emission factors (Table S2) from an emission inventory developed by Tsinghua University (Cai et al., 2017; Ding et al., 2019). Besides, we used the survey data of rural coal to electricity in Beijing by our research group. Results show that the wind power generated in the 16-GW scenario could meet electricity demand for 77% of the rural household heating in Beijing,

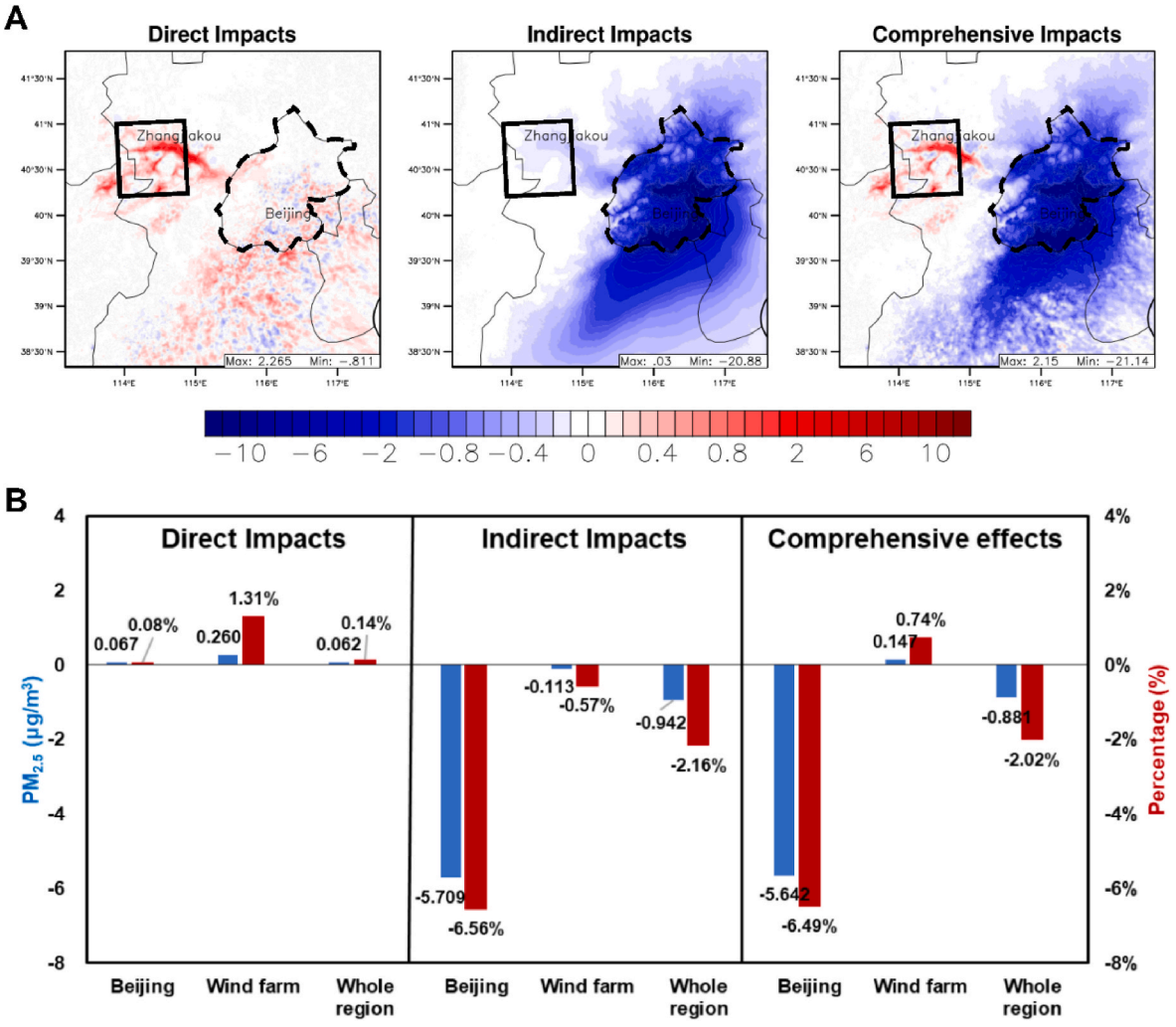


Fig. 6. Monthly average direct, indirect, and comprehensive impacts on $PM_{2.5}$ concentrations: the spatial distributions (A) and absolute values (B) of changes in $PM_{2.5}$ concentrations for designated regions. Blue columns in (B) represent the monthly average effect in different regions, and red columns represent the percentage of the impacts compared to total average concentrations. (For interpretation of the references to color in this figure legend, the reader is referred to the Web version of this article.)

and reduce 64% of air pollutants and CO_2 emissions by replacing coal-heating. The total reduced emissions are 1.56, 0.94, 3.15, 2.45 and 1001.00 kt for SO_2, NO_x, primary PM_{10}, primary $PM_{2.5}$, and CO_2, respectively. The indirect impacts to $PM_{2.5}$ concentrations through substituting wind power for coal to provide rural heat in Beijing are evident, resulting in monthly average decreases of 5.709 μg/m^3 (6.56%) in the Beijing area, 0.113 μg/m^3 (0.57%) in the wind farm area and 0.942 μg/m^3 (2.16%) in the entire study domain. The combination of the indirect and direct (i.e., comprehensive) impacts leads to net increases of $PM_{2.5}$ concentrations of only 0.147 μg/m^3 (0.72%) in the wind farm area, but sizable reductions of 5.642 μg/m^3 (6.49%) in the Beijing area and 0.881 μg/m^3 (2.02%) in the study domain (Fig. 6B).

4. Discussion

We further considered the relationship between the direct air quality changes and the distribution of population. Fig. 7A and B indicate that areas directly impacting $PM_{2.5}$ are concentrated mainly in lower population density regions in Beijing and wind farm areas, including an overall increase in $PM_{2.5}$ in the wind farm area. To characterize the impacts on $PM_{2.5}$ and exposed population, Fig. 7C depicts the changes in population-weighted exposure (PWE) (Zhao et al., 2018), which indicates that when considering the population density, the direct impacts on $PM_{2.5}$ in the wind farm area (increased 0.563 μg/m^3) are still larger than for Beijing (increased 0.059 μg/m^3).

The comprehensive impacts of the wind farm operation and electric replacement displayed in Fig. 6A illustrate an expected increase in $PM_{2.5}$ in the wind farm local area with a decrease in the Beijing region, which raises a concern about the unfairness of regional policies (Fang et al., 2019): to achieve regional air quality goals, dispatch of wind power will lead to improvement of air quality in the more spacious target area but also change the local meteorology and increase air pollution concentrations in the wind farm local area. These results imply that given the uneven distribution of urban agglomerations, investments in wind power resources and regional environmental policies may tend to sacrifice the interests of residents in the wind farm area. To eliminate or reduce this unfairness, it is critical to coordinate regional policies, such as allocating wind power to rural residents using coal in the ZJK area.

We realize that even with better knowledge of energy processes involved with flow of air over complex terrains and associated improvements in the meteorological model, its ability to deal with the impact of complex orography will continue to have limitations as compared with the treatment of flow over plains regions (Serafin et al., 2018). To ensure the accuracy of our mountain simulation, we compared our results for wind speed and temperature with data from radiosonde observations in the mountainous region (Fig. S3). The coefficients of determination of wind speed and temperature by fitting straight lines are 0.95 and 0.99 respectively, which meets statistical standards and indicates reasonable accuracy of our simulation. In terms of scenario design, we set up an idealized distribution of wind turbines which differs from the realistic placement of wind farms. Thus, there is still a gap between the potential impact of this research and operational reality. To explore the effect of different WF distributions and make our results more convincing, we present in Fig. S7 the trend projected due to a potential increase in deployment of wind power from 8 GW to 32 GW. These results also support our analysis of the impacts presented in this research. In addition, we realize that the assessment of wind power deployment of the air pollution impacts is still not comprehensive enough. Because, in the scenario design, we only choose the maximum benefits of electricity substitution sector to evaluate the indirect impacts of wind power (Wang et al., 2020). However, as the electrification process accelerates, the use of clean energy will more effectively improve the quality of the atmospheric environment from the source to the end-of-pipe. And the indirect benefits brought by the deployment and transmission of large-scale wind power will inevitably exceed the absolute impact of the simulation in this paper.

5. Conclusion

In our study, we linked meteorological changes from operated wind farms with air quality impacts, and we discussed for the first time the comprehensive effects of the deployment of wind power on air pollution in BTH in China. We find that the operating wind farms have almost negligible monthly average direct meteorological influences on the distribution of air pollutants in both the local and downstream regions. Moreover, the direct impacts of wind farms on $PM_{2.5}$ can be attributed to the overall effects of decreased horizontal advection and increased vertical dispersion. However, at some specific moments, such as during heavy pollution periods, the direct impacts of $PM_{2.5}$ can reach 6–8 μg/m^3, and the disturbance of the wind farms has brought both positive and negative states to the downwind region. Thus, wind farm maintenance is scheduled during the pollution periods to avoid the short-term non-negligible adverse influences.

In terms of indirect energy substitution effects, the results suggest conspicuous benefits realized in coal-to-wind power substitution for residential energy in rural Beijing areas. These comprehensive results also remind us that we should consider the environmental unfairness brought by energy conversion and application and that even renewable energy might bring forth corresponding consequences on the local area. Therefore, it is necessary to coordinate feasible applications in green wind power with considerations of maximizing environmental benefits.

CRediT authorship contribution statement

Ziwen Ruan: Conceptualization, Methodology, Data curation, Formal analysis, Writing – original draft. **Xi Lu:** Conceptualization, Methodology, Formal analysis, Writing – review & editing. **Shuxiao Wang:** Methodology, Resources, Software. **Jia Xing:** Methodology,

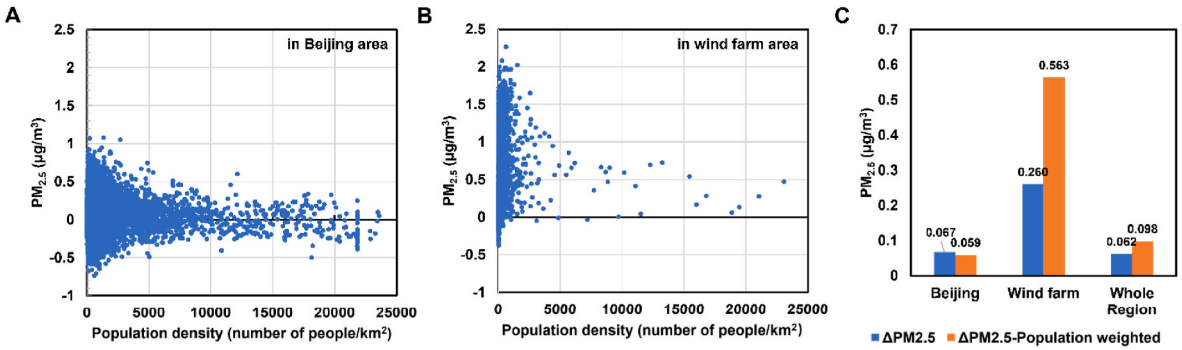


Fig. 7. The monthly average direct impacts on $PM_{2.5}$ concentrations compared with population densities in Beijing (A) and wind farm (B) areas, and population-weighted exposure (C).

Software, Formal analysis, Writing – review & editing. **Wei Wang:** Methodology. **Dan Chen:** Conceptualization, Methodology, Formal analysis, Writing – review & editing. **Chris P. Nielsen:** Formal analysis, Writing – review & editing. **Yong Luo:** Validation. **Kebin He:** Resources. **Jiming Hao:** Resources.

Declaration of competing interest

The authors declare that they have no known competing financial interests or personal relationships that could have appeared to influence the work reported in this paper.

Acknowledgements

This work was supported by the National Key R&D Program (2016YFC0208901), the National Natural Science Foundation of China (No. 72025401, 71722003, 71974108, and 71690244), Tsinghua University-INDITEX Sustainable Development Fund, and Tsinghua University-Center of High Performance Computing.

Appendix A. Supplementary data

Supplementary data to this article can be found online at https://doi.org/10.1016/j.atmosenv.2022.119074.

References

Ancell, B.C., Bogusz, A., Lauridsen, M.J., Nauert, C.J., 2018. Seeding chaos: the dire consequences of numerical noise in NWP perturbation experiments. Bull. Am. Meteorol. Soc. 99, 615–628.
Archer, C.L., Wu, S., Vasel-Be-Hagh, A., Brodie, J.F., Delgado, R., St Pé, A., Oncley, S., Semmer, S., 2019. The VERTEX field campaign: observations of near-ground effects of wind turbine wakes. J. Turbul. 20, 64–92.
Archer, C., Wu, S., Ma, Y., Jimenez, P., 2020. Two corrections for turbulent kinetic energy generated by wind farms in the WRF model. Mon. Weather Rev. 148, 4823–4835.
Blahak, U., Goretzki, B., Meis, J., 2010. A simple parameterization of drag forces induced by large wind farms for numerical weather prediction models. Eur. Wind Energy Conf. Exhib. 6, 186–189, 2010.
Boylan, J.W., Russell, A.G., 2006. PM and light extinction model performance metrics, goals, and criteria for three-dimensional air quality models. Atmos. Environ. 40, 4946–4959.
Byun, D.W., Ching, J.K.S., 1999. Science Algorithms of the EPA Models-3 Community Multiscale Air Quality (CMAQ) Modeling System. US Environmental Protection Agency EPA/600/R-99/030, p. 150.
Byun, D.W., Pleim, J.E., Tang, R.T., Al, B., 1999. Meteorology-chemistry Interface Processor (MCIP) for Models-3 Community Multiscale Air Quality (CMAQ) Modeling System. US Environmental Protection Agency EP A/600/R-99/030, pp. 1–90.
Cai, S., Wang, Y., Zhao, B., Wang, S., Chang, X., Hao, J., 2017. The impact of the "air pollution prevention and control action plan" on $PM_{2.5}$ concentrations in jing-jin-ji region during 2012–2020. Sci. Total Environ. 580, 197–209.
Chang, X., Wang, S., Zhao, B., Xing, J., Liu, X., Wei, L., Song, Y., Wu, W., Cai, S., Zheng, H., Ding, D., Zheng, M., 2019. Contributions of inter-city and regional transport to $PM_{2.5}$ concentrations in the Beijing-Tianjin-Hebei region and its implications on regional joint air pollution control. Sci. Total Environ. 660, 1191–1200.
Chen, D., Liu, Z., Fast, J., Ban, J., 2016. Simulations of sulfate–nitrate–ammonium (SNA) aerosols during the extreme haze events over northern China in October 2014. Atmos. Chem. Phys. 16, 10707–10724.
Ding, D., Xing, J., Wang, S., Liu, K., Hao, J., 2019. Estimated contributions of emissions controls, meteorological factors, population growth, and changes in baseline mortality to reductions in ambient $PM_{2.5}$ and $PM_{2.5}$-Related mortality in China, 2013-2017. Environ. Health Perspect. 127, 67009.
Ek, M.B., Mitchell, K.E., Lin, Y., Rogers, E., Tarpley, J.D., 2003. Implementation of NOAH land surface model advances in the NCEP operational mesoscale Eta model. J. Geophys. Res. Atmos. 108, 8851.
Emery, C., Tai, E., Yarwood, G., 2001. Enhanced Meteorological Modeling and Performance Evaluation for Two texas Ozone Episodes. Final Report Submitted to Texas Natural Resources Conservation Commission.
Environmental Protection Agency, U.S, 2007. Guidance on the Use of Models and Other Analyses for Demonstrating Attainment of Air Quality Goals for Ozone, $PM_{2.5}$, and Regional Haze. EPA -454/B-07-002.
Fang, D., Chen, B., Hubacek, K., Ni, R., Chen, L., Feng, K., Lin, J., 2019. Clean air for some: unintended spillover effects of regional air pollution policies. Sci. Adv. 5, 1–10.
Fitch, A.C., Olson, J.B., Lundquist, J.K., Dudhia, J., Gupta, A.K., Michalakes, J., Barstad, I., 2012. Local and mesoscale impacts of wind farms as parameterized in a mesoscale NWP model. Mon. Weather Rev. 140, 3017–3038.
Fitch, A.C., Lundquist, J.K., Olson, J.B., 2013. Mesoscale influences of wind farms throughout a diurnal cycle. Mon. Weather Rev. 141, 2173–2198.
Harris, R.A., Zhou, L., Xia, G., 2014. Satellite observations of wind farm impacts on nocturnal land surface temperature in Iowa. Rem. Sens. 6.
Hong, S.Y., Lim, J., 2006. The WRF single-moment 6-class Microphysics scheme (WSM6). Asia Pac. J. Atmos. Sci. 42, 129–151.
Hu, J., Chen, J., Ying, Q., Zhang, H., 2016a. One-year simulation of ozone and particulate matter in China using WRF/CMAQ modeling system. Atmos. Chem. Phys. Discuss. 1–31.
Hu, J., Wang, P., Ying, Q., Zhang, H., Chen, J., Ge, X., Li, X., Jiang, J., Wang, S., Zhang, J., Zhao, Y., Zhang, Y., 2016b. Modeling biogenic and anthropogenic secondary organic aerosol in China. Atmos. Chem. Phys. Discuss. 1–31.
Hu, R., Wang, S., Zheng, H., Zhao, B., Liang, C., Chang, X., Jiang, Y., Yin, R., Jiang, J., Hao, J., 2021. Variations and Sources of Organic Aerosol in Winter Beijing under Markedly Reduced Anthropogenic Activities during COVID-2019. Environmental Science & Technology.
Iacono, M.J., Delamere, J.S., Mlawer, E.J., Shephard, M.W., Clough, S.A., Collins, W.D., 2008. Radiative forcing by long-lived greenhouse gases:Calculations with the AER radiative transfer models. J. Geophys. Res. 113, 1–8.
Kain, J.S., Kain, J., 2004. The Kain - fritsch convective parameterization: an update. J. Appl. Meteorol. 43, 170–181.
Keith, D.W., Decarolis, J.F., Denkenberger, D.C., Lenschow, D.H., Malyshev, S.L., Pacala, S., Rasch, P.J., 2004. The influence of large-scale wind power on global climate. Proc. Natl. Acad. Sci. U. S. A. 101, 16115–16120.
Li, Y., Kalnay, E., Motesharrei, S., Rivas, J., Kucharski, F., Kirk-Davidoff, D., Bach, E., Zeng, N., 2018. Climate model shows large-scale wind and solar farms in the Sahara increase rain and vegetation. Science 361, 1019–1022.
Li, H., Jiang, H., Dong, K., Wei, Y., Liao, H., 2019a. A comparative analysis of the life cycle environmental emissions from wind and coal power: evidence from China. J. Clean. Prod. 248, 119192.
Li, X., Hu, X., Ma, Y., Wang, Y., Li, L., Zhao, Z., 2019b. Impact of planetary boundary layer structure on the formation and evolution of air-pollution episodes in Shenyang, Northeast China. Atmos. Environ. 214, 116850.
Li, S., Huang, T., Mo, J., Li, J., Zhang, X., Du, J., Tao, S., Liu, J., Jiang, W., Lian, L., Gao, H., Mao, X., Zhao, Y., Ma, J., 2020. Do large-scale wind farms affect air quality forecast? Modeling evidence in Northern China. Atmos. Chem. Phys. Discuss. 2020, 1–35.
Lu, X., Zhang, S., Xing, J., Wang, Y., Chen, W., Ding, D., Wu, Y., Wang, S., Duan, L., Hao, J., 2020. Progress of air pollution control in China and its challenges and opportunities in the ecological civilization era. Engineering 6, 1423–1431.
Ma, Z., Xue, B., Geng, Y., Ren, W., Fujita, T., Zhang, Z., Puppim de Oliveira, J.A., Jacques, D.A., Xi, F., 2013. Co-benefits analysis on climate change and environmental effects of wind-power: a case study from Xinjiang, China. Renew. Energy 57, 35–42.
Miller, L.M., Keith, D.W., 2018. Climatic impacts of wind power. Joule 2, 2618–2632.
Mo, J., Huang, T., Zhang, X., Zhao, Y., Liu, X., Li, J., Gao, H., Ma, J., 2017. Spatiotemporal distribution of nitrogen dioxide within and around a large-scale wind farm – a numerical case study. Atmos. Chem. Phys. 17, 14239–14252.
Nakanishi, M., Niino, H., 2009. Development of an improved turbulence closure model for the atmospheric boundary layer. J. Meteorol. Soc. Jpn. 87, 895–912.
Nordman, E.E., Vandermolen, J., 2014. Wind Power and Air Quality: Reducing Air Pollution and Carbon Emissions in Michigan.
Raadal, H.L., Vold, B.I., Myhr, A., Nygaard, T.A., 2014. GHG emissions and energy performance of offshore wind power. Renew. Energy 66, 314–324.
Rajewski, D.A., Takle, E.S., Lundquist, J.K., Oncley, S., Prueger, J.H., Horst, T.W., Rhodes, M.E., Pfeiffer, R., Hatfield, J.L., Spoth, K.K., Doorenbos, R.K., 2013. Crop wind energy experiment (CWEX): observations of surface-layer, boundary layer, and mesoscale interactions with a wind farm. Bull. Am. Meteorol. Soc. 94, 655–672.
Rajewski, D.A., Takle, E.S., Lundquist, J.K., Prueger, J.H., Pfeiffer, R.L., Hatfield, J.L., Spoth, K.K., Doorenbos, R.K., 2014. Changes in fluxes of heat, H_2O, and CO_2 caused by a large wind farm. Agric. For. Meteorol. 194, 175–187.
Roy, S.B., Traiteur, J.J., 2010. Impacts of wind farms on surface air temperatures. Proc. Natl. Acad. Sci. U. S. A. 107, 17899–17904.
Serafin, S., Adler, B., Cuxart, J., De Wekker, S., Gohm, A., Grisogono, B., Kalthoff, N., Kirshbaum, D., Rotach, M., Schmidli, J., Stiperski, I., Večenaj, Ž., Zardi, D., 2018. Exchange processes in the atmospheric boundary layer over mountainous terrain. Atmosphere 9, 32.
Skamarock, W.C., Klemp, J.B., Dudhia, J., Gill, D.O., Barker, D.M., Duda, M.G., Huang, X. Y., Wang, W., Powers, J.G., 2008. A description of the advanced research WRF Version 3. In: NCAR Tech. Note NCAR/TN-4751STR, p. 105.
Slawsky, L.M., Zhou, L., Roy, S.B., Xia, G., Vuille, M., Harris, R.A., 2015. Observed thermal impacts of wind farms over northern Illinois. Sensors 15.
Smith, C.M., Barthelmie, R.J., Pryor, S.C., 2013. In situ observations of the influence of a large onshore wind farm on near-surface temperature, turbulence intensity and wind speed profiles. Environ. Res. Lett. 8, 034006.
Tao, H., Xing, J., Zhou, H., Chang, X., Li, G., Chen, L., Li, J., 2018. Impacts of land use and land cover change on regional meteorology and air quality over the Beijing-Tianjin-Hebei region, China. Atmos. Environ. 189, 9–21.
Tao, H., Xing, J., Zhou, H., Pleim, J., Ran, L., Chang, X., Wang, S., Chen, F., Zheng, H., Li, J., 2019. Impacts of improved modeling resolution on the simulation of meteorology, air quality, and human exposure to $PM_{2.5}$, O_3 in Beijing, China. J. Clean. Prod. 243, 118574.
Tao, H., Xing, J., Pan, G., Pleim, J., Ran, L., Wang, S., Chang, X., Li, G., Chen, F., Li, J., 2021. Impact of anthropogenic heat emissions on meteorological parameters and air quality in Beijing using a high-resolution model simulation. Front. Environ. Sci. Eng. 16.

Tu, Q., Betz, R., Mo, J., Fan, Y., Liu, Y., 2019. Achieving grid parity of wind power in China – present levelized cost of electricity and future evolution. Appl. Energy 250, 1053–1064.
Walsh-Thomas, J.M., Cervone, G., Agouris, P., Manca, G., 2012. Further evidence of impacts of large-scale wind farms on land surface temperature. Renew. Sustain. Energy Rev. 16, 6432–6437.
Wang, S., Zhao, B., Cai, S., Klimont, Z., He, K., 2013. Emission trends and mitigation options for air pollutants in East Asia. Atmos. Chem. Phys. 14, 2601–2674.
Wang, J., Wang, S., Jiang, J., Ding, A., Zheng, M., Zhao, B., Wong, D.C., Zhou, W., Zheng, G., Wang, L., Pleim, J.E., Hao, J., 2014. Impact of aerosol–meteorology interactions on fine particle pollution during China's severe haze episode in January 2013. Environ. Res. Lett. 9.
Wang, Q., Luo, K., Wu, C.L., Fan, J.R., 2019a. Impact of substantial wind farms on the local and regional atmospheric boundary layer: case study of Zhangbei wind power base in China. Energy 183, 1136–1149.
Wang, Q., Luo, K., Yuan, R.Y., Zhang, S.X., Fan, J.R., 2019b. Wake and performance interference between adjacent wind farms: case study of Xinjiang in China by means of mesoscale simulations. Energy 166, 1168–1180.
Wang, Y., Wang, S., Song, F., Yang, J., Zhu, J., Zhang, F., 2020. Study on the forecast model of electricity substitution potential in Beijing-Tianjin-Hebei region considering the impact of electricity substitution policies. Energy Pol. 144, 111686.
Wang, J., Xing, J., Wang, S., Mathur, R., Wang, J., Zhang, Y., Pleim, J., Ding, D., Chang, X., Jiang, J., Zhao, P., Sahu, S., Jin, Y., Wong, D., Hao, J., 2022. The Pathway of Aerosol Direct Effects Impact on Secondary Inorganic Aerosol Formation.
Xi, J., 2020. Building on Past Achievements and Launching a New Journey for Global Climate Actions. Xinhua.
Xia, G., Zhou, L., Freedman, J.M., Roy, S.B., Harris, R.A., Cervarich, M.C., 2016. A case study of effects of atmospheric boundary layer turbulence, wind speed, and stability on wind farm induced temperature changes using observations from a field campaign. Clim. Dynam. 46, 2179–2196.
Xu, L., Pang, M., Zhang, L., Poganietz, W.-R., Marathe, S.D., 2018. Life cycle assessment of onshore wind power systems in China. Resour. Conserv. Recycl. 132, 361–368.
Yang, J., Song, D., Wu, F., 2017. Regional variations of environmental co-benefits of wind power generation in China. Appl. Energy 206, 1267–1281.
Yang, X., Pakula, M., Sotiropoulos, F., 2018. Large-eddy simulation of a utility-scale wind farm in complex terrain. Appl. Energy 229, 767–777.
Zhang, S., Wei, J., Chen, X., Zhao, Y., 2020. China in global wind power development: role, status and impact. Renew. Sustain. Energy Rev. 127.
Zhang, C., Lu, X., Ren, G., Chen, S., Hu, C., Kong, Z., Zhang, N., Foley, A.M., 2021. Optimal allocation of onshore wind power in China based on cluster analysis. Appl. Energy 285, 116482.
Zhao, B., Zheng, H., Wang, S., Smith, K.R., Lu, X., Aunan, K., Gu, Y., Wang, Y., Ding, D., Xing, J., Fu, X., Yang, X., Liou, K.N., Hao, J., 2018. Change in household fuels dominates the decrease in $PM_{2.5}$ exposure and premature mortality in China in 2005-2015. Proc. Natl. Acad. Sci. U. S. A. 115, 12401–12406.
Zhao, B., Zhao, J., Zha, H., Hu, R., Liu, Y., Liang, C., Shi, H., Chen, S., Guo, Y., Zhang, D., Aunan, K., Zhang, S., Zhang, X., Xue, L., Wang, S., 2021. Health benefits and costs of clean heating renovation: an integrated assessment in a major Chinese city. Environ. Sci. Technol. 55, 10046–10055.
Zheng, H., Zhao, B., Wang, S., Wang, T., Ding, D., Chang, X., Liu, K., Xing, J., Dong, Z., Aunan, K., Liu, T., Wu, X., Zhang, S., Wu, Y., 2019. Transition in source contributions of $PM_{2.5}$ exposure and associated premature mortality in China during 2005-2015. Environ. Int. 132, 105111.
Zhou, L., Tian, Y., Roy, B.S., Thorncroft, C., Bosart, L.F., Hu, Y., 2012. Impacts of wind farms on land surface temperature. Nat. Clim. Change 2, 539–543.
Zhou, L., Tian, Y., Baidya Roy, S., Dai, Y., Chen, H., 2013. Diurnal and seasonal variations of wind farm impacts on land surface temperature over western Texas. Clim. Dynam. 41, 307–326.
, Global Wind Report. https://gwec.net/global-wind-report-2021/.